J Mater Sci: Mater Electron

UV detector characteristics of ZnO thin film deposited on Corning glass substrates using low-cost fabrication method

N. M. Abd-Alghafour[1,*], Imad H. Kadhim[2], and Ghassan Adnan Naeem[3]

[1] Iraqi Ministry of Education, Al-Anbar, Biophysics Department, College of Applied Sciences-HIT, University of Anbar, Radami 31007, Iraq
[2] Ministry of Education, Iraq, Baghdad 11800, Iraq
[3] Biophysics Department, College of Applied Science-HIT, University of Anbar, Radami 31007, Iraq

Received: 28 June 2021
Accepted: 15 October 2021

ABSTRACT

A UV detector based on the zinc oxide (ZnO) thin film was fabricated by using sol–gel process with zinc acetate dehydrate ($Zn(CH_3COO)_2 2H_2O$) as a precursor. The hexagonal crystal structure of the ZnO sample was revealed by X–ray diffraction patterns (XRD). Field emission scanning electron microscopy (FESEM) results indicated that the ZnO film's surface is smooth and uniform, having grain size of about 50 nm. Photoluminescence spectroscopy (PL) revealed UV light and broadband emissions, which were attributed to near band–edge (NBE) and deep level–edge emissions (DLE), respectively. The metal–semiconductor–metal (MSM) device based on the fabricated ZnO film showed a sensitivity of 43% upon exposure light (0.66 μW/cm^2) at 5 V and a response peak of 4.3 A/W upon exposure to UV light, respectively. The UV detector showed excellent stability with time and a strong photocurrent response under 380 nm light. These results show a low-cost method of fabricating a high-performance ZnO MSM UV photodetector with a quick response, fast recovery, and high responsivity.

1 Introduction

In the recent, researchers are trying to build up high-performance photodetectors by using wide band-gap semiconductors such as SnO_2, WO_3, NiO, MoO_3, ZnO etc. [1, 2]. Among these, ZnO thin film has a wide and optical band gap of 3.37 eV at ambient temperature with the hexagonal wurtzite structure [3–5]. In addition, it possesses a substantially higher binding exciton potential (60 meV) as compared to other materials such as gallium nitride (GaN) (20 meV) at room temperature [3]. ZnO has provided many advantages like high photosensitivity, non-toxicity, and low cost [6]. Hence, ZnO film is extremely useful for a wide range of engineering applications, including chemical sensors, biosensors, pH sensors,

Address correspondence to E-mail: nabeel.ma@uoanbar.edu.iq

https://doi.org/10.1007/s10854-021-07252-z
Published online: 28 October 2021

light-emitting sensors, and UV detectors [7]. ZnO thin film can be deposited via different processes, such as chemical vapor deposition [8], magnetron sputtering method [9], molecular beam techniques [10], spray pyrolysis technique [11], and sol–gel coating method [12]. ZnO films deposition by sol–gel method has been largely investigated in the past [13]. The sol–gel process offers several advantages over others methods, including low reaction temperature, simple procedure, and inexpensive cost [14]. Because it is extremely effective at creating thin films, the sol–gel approach has emerged as one of the most promising processing routes, to form transparent, uniform, multi–component oxide films with a wide range of compositions on a variety of substrates at low cost.

Numerous research groups are interested in obtaining high-quality ZnO thin films in optoelectronic applications. The UV photodetector based on ZnO has unique advantages that possess high sensitivity and responsivity. However, the performance of the ZnO UV photodetector is based upon its structural and optical properties. Mun et al. [15] fabricated ZnO flexible UV photodetector (PDs) on the flexible polydimethylsiloxane (PDMS) by using water-soluble sacrificial (NaCl) crystals. The influence of tensile stress on the PDs performance was investigated. The photocurrent increased to 2.5 pA under UV light, while the off-current was 0.6 pA, resulting in a UV on/off photocurrent ratio of 4.2 at applied bias voltage of 5 V. Yadav et al. [16] prepared ZnO film via using RF-sputtering method. ZnO thin film that indicated high responsivity of 8.57 kA/W and the sensitivity of 31.3×10^3. The enhanced photo-response of ZnO thin films was related to changes in the surfaces conductivity of the film due to the induced electric charge. Panda et al. [17] deposited ZnO thin films onto glass substrates via using thermal evaporation technique for application as UV sensor. The maximum value of the photocurrent gain was 2, attributed to annealing process. Hanna et al. [18] developed a visible-blind UV detector based on the ZnO films at zero applied bias voltages. The results indicated that the responsivity and quantum efficiency of the film at 5 V under 360 nm light illumination were 0.037 A/W and 12.86%, respectively. Pon et al. [19] fabricated UV detector based on the ZnO thin films via using cost-effective nebulizer spray pyrolysis process. The device demonstrated significantly higher selectivity of about 1.22×10^{10} Jones at peak wavelength of 390 nm. ZnO thin films showed extremely responsivity of 0.38 m A/W. ZnO thin film indicated a good candidate for photodetector applications. Ali et al. [20] investigated UV photodetectors based on the ZnO thin film. Thin film was deposited on silicon substrates via using thermal evaporation method. The device showed a good sensitivity and efficiency upon reverse applied voltage. Conversely, the UV detection sensitivity decreased proportionally under forward bias voltage.

In this study, sol–gel coating method was used to deposit ZnO thin films using zinc acetate dehydrate ($Zn(CH_3COO)_2{\cdot}2H_2O$) solution onto Corning glass substrates. The solution concentration was used form 0.5 M. The aim of this research is to create a UV detector on a low-cost substrate with a quick response, fast recovery, and high responsivity.

2 Experimental details

2.1 Synthesis of ZnO thin film

ZnO thin film was deposited onto Corning glass substrates via using sol–gel method. The reaction mixture was produced utilizing zinc acetate dehydrate and ethanol-ethanolamine ($NH_2CH_2CH_2OH$) as solution and stabilizer, respectively. The concentrations of the zinc acetate dehydrate and ethanol ethanolamine were varied between 0.5 and 1 M, with a 1:1 molarity of zinc acetate dehydrate ethanolamine. The mixture of solution was stirred at ambient temperature for 1 h by using a 3000 rpm magnetic stirrer. Finally, before the solution was spin coated on the Corning glass substrate, the substrate was aged for 3 days. The deposition was conducted utilizing a spin coater of 60 s with a speed of 3000 rpm. ZnO thin film was pre-annealed for 1 h after coating at 150 °C. To achieve the crystallization of the thin films, ZnO film was annealed in air at 350 °C for 2 h. The structural characteristics of the film were examined using an X-ray diffractometer (PANalytical X'Pert PRO) equipped with Cu-Kα a radiation (λ = 1.5418 Å). The morphological characteristics were studied via using a field emission scanning electron microscopy (FESEM) model (FEI/Nova Nano SEM450) with energy-dispersive X-ray spectroscopy (EDX). The optical characteristics were performed using a photoluminescence (PL) spectroscopy (Jobin Yvon HR800 UV, Edison, NJ, USA)

with a He-Cd laser (325 nm, 20 mW). As determined by the optical reflectometer (Filmetrics F20), the thickness of the ZnO thin film is calculated to be in the range of 150 nm–200 nm. Using a computer-controlled integrated source meter (Keithley 2400) at room temperature, the current–voltage (*I-V*) measurements were obtained. Using light filters, spectral responsivity measurements were taken out at different wavelengths. All the tests were carried out under atmospheric conditions at room temperature.

2.2 Device fabrication

The UV detector device was manufactured by depositing 120 nm thickness of platinum (pd) grid as the front connection on the top of ZnO film at 650 °C using a metal mask in the presence of junctions. There were two conductive contacts (electrodes) with a five fingers each in the contact metal structure. The length and width of each finger were 3.4 mm and 0.35 mm with a distance of 0.4 mm between the two fingers. The shadow mask's structure and dimensions are shown in Fig. 1a. By using DC-magnetron RF-sputtering system at ambient temperature, the electrodes were deposited; the power was fixed at 120 W with an evacuation force less than 3×10^{-5} -mbar. High-purity Ar was used at a fixed ratio of 17%. Figure 1b displays schematic a diagram of UV semiconductor devices structure. The active area was found to be 0.25 cm^2.

2.3 Mechanism of photodetection

The photodetection in the ZnO thin film is mainly produced via desorption and adsorption processes of the oxygen molecules on the film surface [21]. The energy band structure of a ZnO thin film under dark condition and under UV irradiation condition is shown schematically in the Fig. 2a, b. When an external voltage is given to the sensor, O_2 should be adsorbed at the surface of the dense diffusion layer material [22]. The oxygen molecules are primarily adsorbed onto the surface of the film layer in dark conditions, then, as illustrated in the Fig. 2a, the oxygen molecules capture the free electrons, which can be summarized as follows:

$$O_{2(g)} + e^- \rightarrow O^-_{(2(ad))} \quad (1)$$

As a result of the oxygen ions, a depletion area is formed, reducing the conductivity of ZnO film. In contrast, electron–hole pairs (e^-–h^+) are formed in ZnO thin-film layer [23] under UV illumination with higher photon energy (hv) than the band gap of the ZnO ($hv \leq E_g$), as follows:

$$hv \rightarrow e^- + h^+ \quad (2)$$

A local electric field separates the (e^-–h^+) pairs in zone of the depletion. The holes (h^+) are moved towards to the film surface by the electric field, where they recombine with electrons from the adsorbed oxygen ions. As illustrated in the Fig. 2b, this condition leads to the release of the oxygen atoms from film surface, which can be summarized as follows:

$$h^+ + O^-_{(2(ad))} \rightarrow O^-_{2(g)} \quad (3)$$

At same time, photo-generated electrons contribute to photoconduction by filling the conduction band (CB). As a result, a rise in the number of electrons leads to a rise in conductivity [24]. As an outcome,

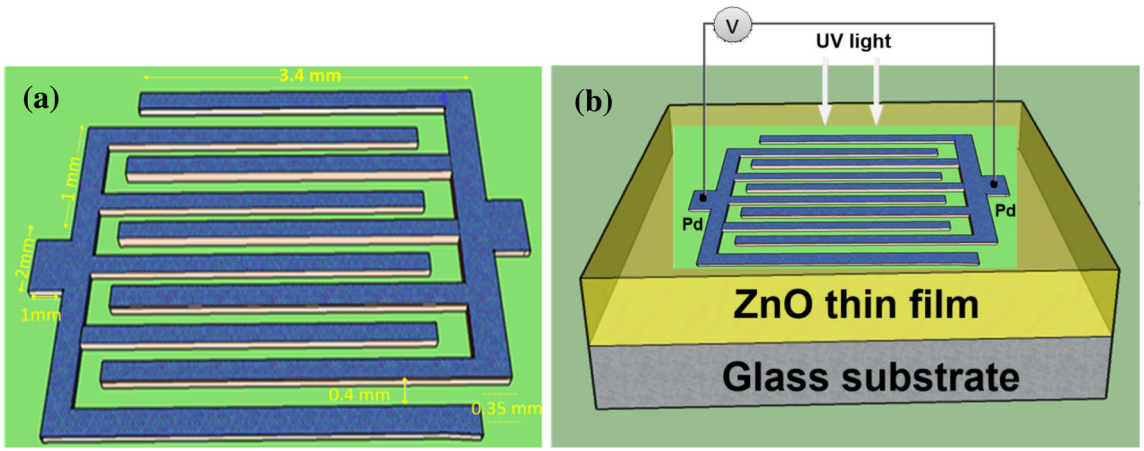

Fig. 1 **a** Schematic of the metal shadow used for the fabrication of MSM-structured UV detector and **b** fabricated ZnO-based UV detector

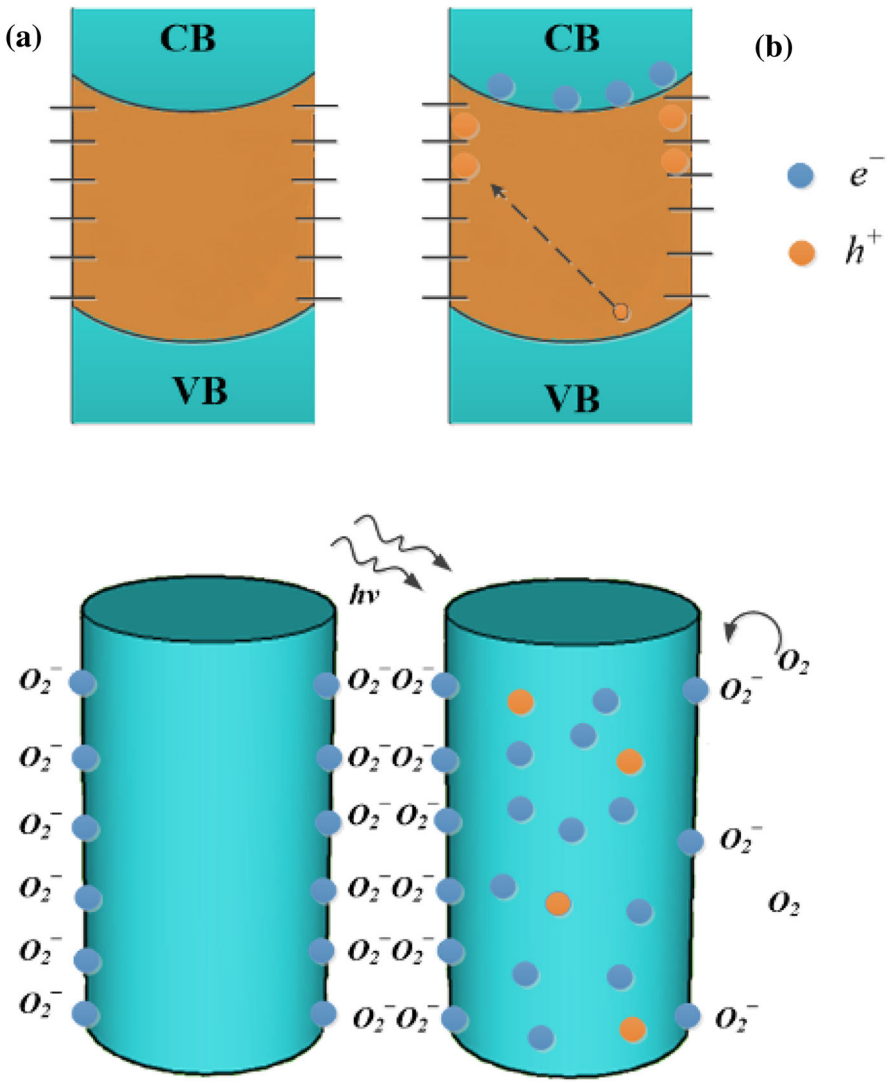

Fig. 2 **a**, **b** Photoconduction in ZnO thin film and energy band diagram **a** under dark condition, and **b** Under UV light illumination

the significant photocurrent measured can be related to the light-induced charge carrier production in the depletion zone [25].

3 Results and discussion

3.1 Structural properties

Figure 3a–c displays XRD patterns of the ZnO thin film with as-grown prepared onto Corning glass substrate via using sol–gel technique. XRD peaks show that three major peaks of the diffraction correspond to the ZnO with planes (100), (002), and (101) corresponding to $2\theta = 34.45°$, 36.16°, and 47.52° comparable to JCPDS card No. 36-1451 [5]. The results indicated that ZnO film is polycrystalline in nature and has a hexagonal wurtzite crystal structure [26]. Further study of the XRD patterns demonstrates that the prefer orientation towards the growth of crystals is along the plane (002). The c-axis orientation, particularly in the (002) plane, may be a common occurrence in the chemical deposition of ZnO films employing organo-zinc compounds [27]. The preferred orientation is assumed to be due to the reduction of surface energy and internal tension. The result could be associated to the c-orientation of the dominant development of crystals. The increase in the annealing temperature caused ZnO to increase its crystallinity [28]. The peak intensity increases to some amount as the annealing temperature is increased to 350 °C, which is due to increase in the crystallite size of ZnO thin film. This suggested a high preferential value for the thin films c-axis

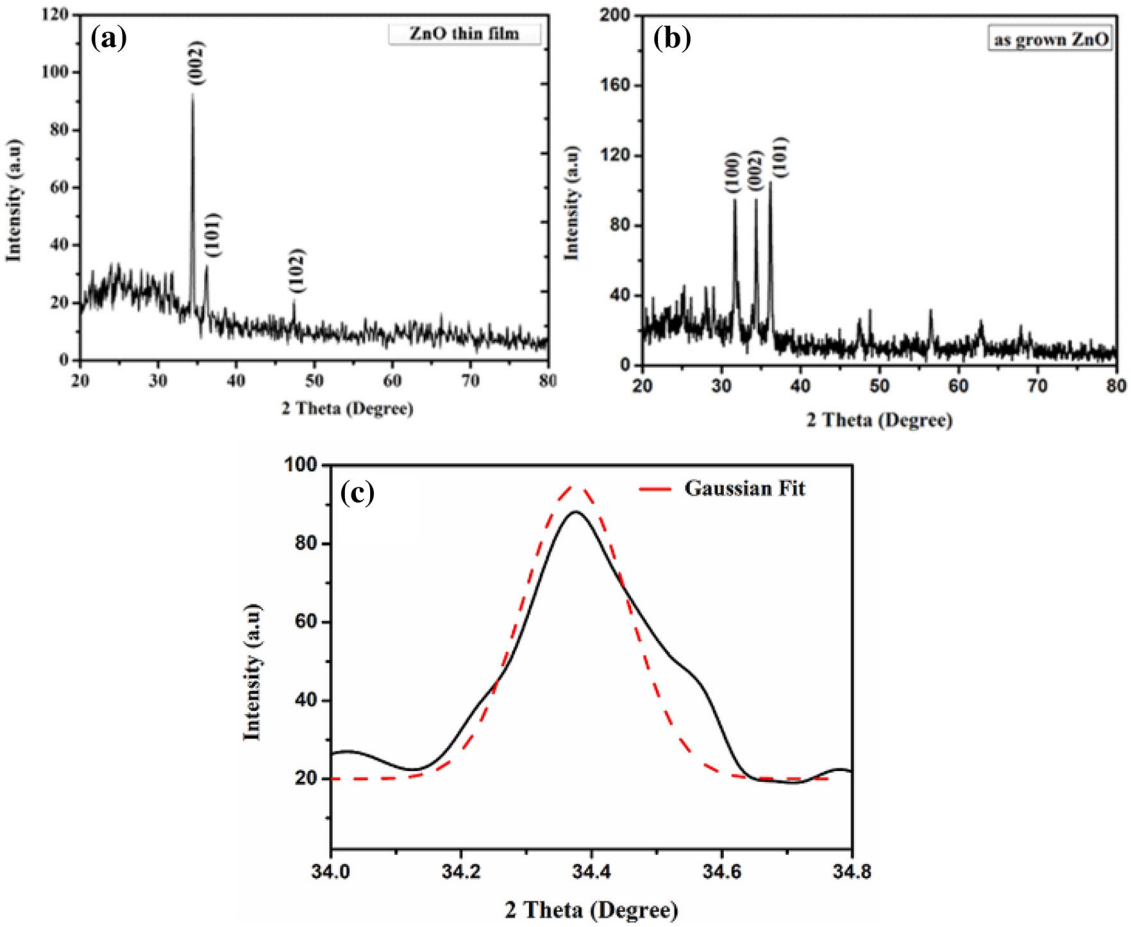

Fig. 3 **a**–**c** X-ray diffraction patterns of ZnO thin film synthesized on Corning glass substrate

direction, aligned perpendicular to the substrate surface. The insufficient supply of thermal energy for recrystallization, grain development, and the powder nature of the films may be to cause for these results [29]. The crystallite sizes (D) of thin film were determined via using the following formula [30]:

$$D = \frac{k\lambda}{\beta_{hkl}\cos\theta}, \tag{4}$$

where D is the average crystallite size, λ is the X-ray wavelength (1.5406 Å); β_{hkl} is full-width at half-maximum (FWHM) (0.189), and θ is XRD diffraction angle (34.375°), respectively. The Scherrer constant is denoted by k. The Scherrer constant is generally $\sim$ 0.9; however, it was later shown that the size of the Scherrer constant is dependent on the shape/geometry of the crystallite. There is uncertainty in k unless the shape/geometry of the crystallites and their distribution are determined. The value k was found to be varying from 0.62 to 2.08 with the actual shape of the crystallites [54]. Figure 3c displays a fitting plot of the XRD results. The new findings are consistent with a recent work that found stress in ZnO along the c-axes and a-axes during deposition when organic chemicals were incorporated into the lattice [31]. The crystallite size was estimated to be 50 nm. The grains tend to combine during annealing, resulting in bigger grains. The decreased FWHM value and higher crystallite size in this case indicate that crystallization is better. When the energy is sufficient to permit the diffusion and recrystallization of the element or compound, the nucleation of small grains into bigger grains happens during annealing treatment [32].

3.2 Morphological properties

The FESEM images with two magnification of ZnO film are shown in Fig. 4a, b. The surface morphology of the films consists of spherical grains that are

uniformly distributed throughout the substrate [33]. It can be seen from the figure that the film's surface annealed at 350 °C is rough with the gully shaped surface, and the grain boundary blurred. It illustrates that the thin film is continuous and packed without voids or porosity. Moreover, no cracking is observed [34]. The production of larger grains from small grains on the ZnO surface was resulted by a rise in substrate temperature, which in turn reduced defect centers and surface defects. Furthermore, because to the coalescence of tiny particles, the mean crystallite size increases as the substrate temperature rises [35]. The particle size measured in an electron microscope is approximately 50 nm, which is in accordance with the XRD results. The EDX analysis was used to evaluate the elementary composition of ZnO film. The results of EDX spectrum are shown in Fig. 4c. The figure shows two peaks corresponding to the elements zinc (Zn) and oxygen (O). The inset of Fig. 4c depicts the compositions of atomic percentage (O = 62.24%, Z = 37.79%) of the constituents of ZnO thin film. The results indicated the purity of the thin film [36].

3.3 Optical properties

Figure 5 displays the photoluminescence spectra (PL) of the prepared ZnO film with laser excitation (He–Cd) source. Two optical bands converge at about 380 nm and 760 nm. The near band-edge (NBE) emission, which is responsible for the recombination of free excitons in ZnO, emits UV approximately 380 nm [37]. The band at wavelength of 760 nm is due to second item diffraction from the grating for band at 380 nm. The violet/blue band at 380 nm can be attributed to a pair of donor–acceptor transitions [38]. The wide band centered at approximately 760 nm with a maximum width of approximately 26.3 nm (FWHM) can be attributed to the transition from the conductive band to oxygen vacancy levels. This can be established that the band gap of ZnO film deposited on glass substrate is similar to band gap of bulk ZnO (E_g = 3.26 eV), which can be correlated with the low level of defects [39].

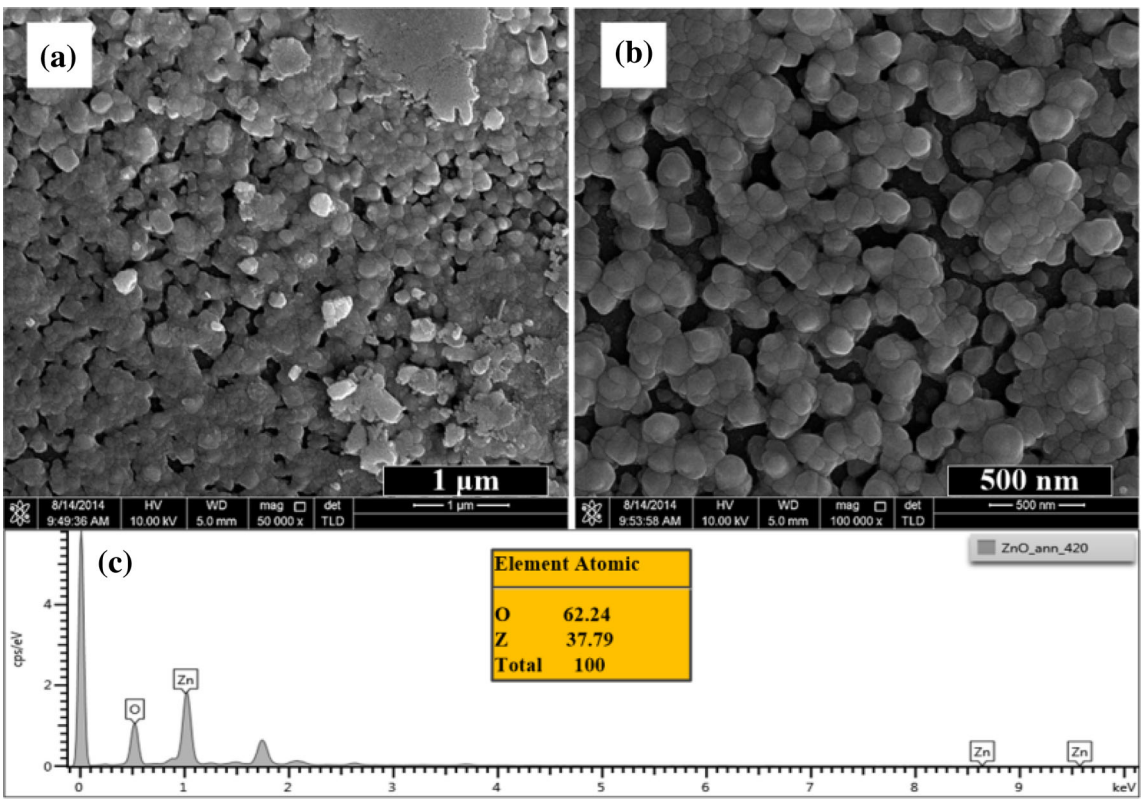

Fig. 4 **a**, **b** FESEM images of ZnO thin film synthesized on glass substrate **c** EDX spectra of ZnO thin film synthesized on glass substrate

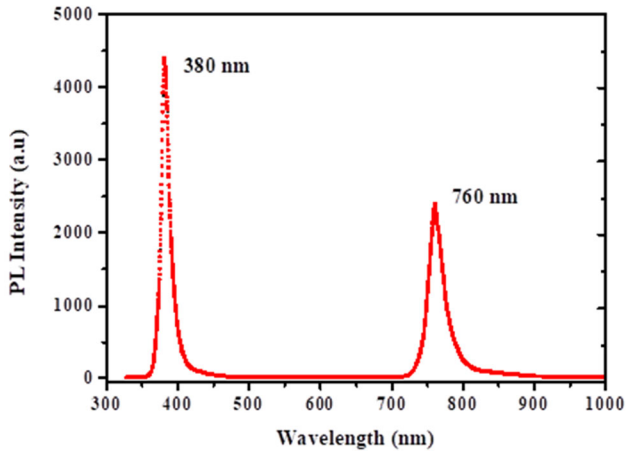

Fig. 5 Photoluminescence spectrum of ZnO thin film synthesized on Corning glass substrate

3.4 UV photodetector application

Figure 6 indicates the *I–V* (current–voltage) diagrams of the UV sensor based on the ZnO thin film under darkness and UV light at wavelength of 380 nm with incident energy of 0.66 μW/cm^2. The light and dark currents are found to be 1.32 μA and 0.83 μA, respectively. It is established that the *I–V* (current–voltage) diagrams are symmetrical and linear, showing the strong Ohmic interaction between ZnO thin film and pd electrodes [40]. The ohmic interaction of the UV detector can be attributed to enhancement of the light-sensitive properties [41]. This improvement of the light–current confirms that the thin film has more photo-excited-free electrons, which is related to higher crystallinity and a substantially prevented recombination of photo-generated carriers. Furthermore, residual contaminants, surface asperities, and asperities all have a significant impact on the electrical contact characteristics.

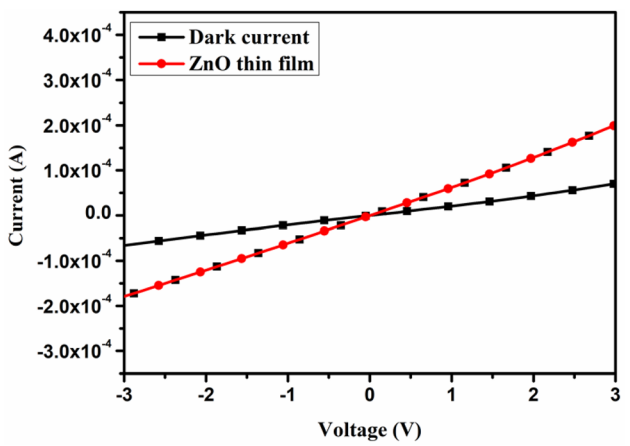

Fig. 6 Dark and illuminated *I–V* characteristics of the ZnO UV sensor device

Figure 7a, b displays the photo-responsivity of UV detector based on the ZnO thin film. The photocurrent rose until it reached 360 nm, after which it drastically fell until it reached 385 nm. The maximum value of response is reported in the range 360 nm–380 nm with the break off-wavelength of 390 nm. The optimum response value of UV detector under light of 385 nm is 4.3 A/W. This greater responsivity can be attributed to ZnO film providing high density with larger and rougher surface areas, as well as the ZnO/glass system forming a good MSM detector. More carriers gathered under illumination in the ZnO thin film can be attributed to the high photocurrent density and responsivity [42]. Because the excitation is proportional to the amount of the excess carriers' generation rate and lifetime, the amount of the observed response is most likely influenced by this. At 390 nm, the cut-off was reached. The progressive cut-off at 385 nm corresponds to the 3.26 eV band-gap energy of ZnO thin film [17]. The light–current decreases dramatically over break off-wavelength, revealing good light sensing of ZnO film for light-blinded UV sensor and these findings are in agreement with PL spectra. This value of UV response exhibits a full-width half-maximum of 20 nm for thin film. This full-width value indicates that ZnO UV detector responds to a very small slight spectral region of light spectrum which means good spectrum selectivity for this detector. The response value of the detector (R) can be defined as the light–current (I_{ph}) generated per light power (P_{in}) on the activity area of detector, which is calculated as follows [43]:

$$R = \frac{I_{ph}(A)}{P_{in}(W)} = \frac{I_{ph}(A)}{E(W/cm^2)A(cm^2)} \quad (5)$$

where E is equal to 0.66 μW/cm^2, which represents the irradiance of the UV light. A is an active area equal to 0.25 cm^2. The high rise in responsivity with applied bias indicates that the photodetector has a large photoconductive gain. UV detector's performance could be improved as a result of ZnO thin film has a high UV responsivity and a large excitation area to volume ratio [44]. It indicates the high surface area of film as well as the existence of the deep level surface trap states within the film, extending the photo-carrier lifetime significantly. Figure 7b

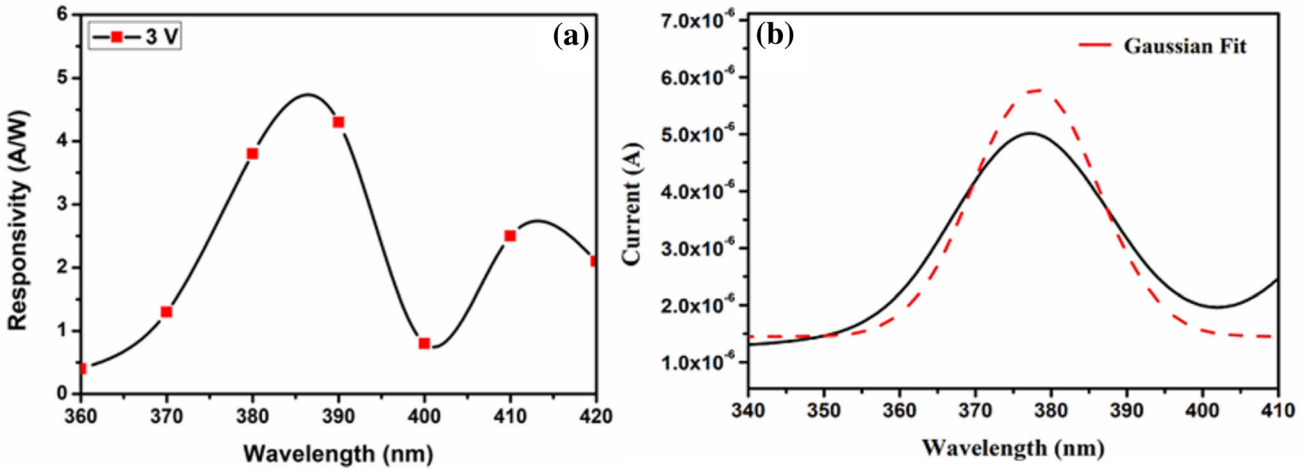

Fig. 7 Spectral responsivity of the ZnO thin-film photodetector

displays a fitting plot of the responsivity results. The following formula can be used to calculate the device's sensitivity (S) to UV radiation:

$$S = \frac{I_{ph} - I_d}{I_d} \times 100. \quad (6)$$

At a 5 V bias, the S value of 43% was tested against UV radiation with a wavelength of 380 nm and an intensity of 0.66 mW/cm^2. The sensitivity improves dramatically when the grain size is lower than the width of the space charge zone or the generated depletion layer.

Figure 8 displays the exchanging behavior of UV detector by controlling the UV light source (incident energy = 0.66 μW/cm^2) at applied bias voltage of 5 V with duration of 20 s. The light–current of the ZnO UV detector increases gradually when the UV illumination is turned on, the light–current of the ZnO UV detector decreased dramatically to its initial stage, showing improved product steadiness and repeatability of detector. The response and recovery times of ZnO UV detector are found 3.7 s and 5.3 s, respectively. This means that sensor with complete transparency is exceptionally apposite for good speed activity due to its excellent UV sensor performance, such as rapid rise and decay times. As shown from Fig. 8, it is seen to that changing in both states (on/off) is flexible and rapid, acting as an extremely effective light-sensitive change. It is found that the dark current is experiencing a small temporal distortion due to the persistent influence of photoconductivity [45]. In the two states (on/off), the calculated photocurrent indicated a steadily increasing value when exposed to UV light and that the current decreased in the dark exponentially. Also, the UV detector can be used to examine the photoresponse with incident light of various wavelengths, various intensities, as studied in the research [46]. As compared to the other values obtained in the literature [20, 45, 47–53] from the ZnO-based UV detector using different methods (Table 1), our ZnO-based UV detector demonstrates relatively better values of UV responsivity and rapid response. The study shows that sol–gel-derived devices exhibit better photo-response as compared to those using thin film deposited by vacuum deposition technique.

4 Conclusion

In this study, ZnO thin film was deposited via using a sol–gel method onto Corning glass substrate. Thin film has a strongly preferred hexagonal wurtzite structure with orientation of the c-axis along (002) plane peak with crystallite size of around 50 nm. The crystalline nature verified the good crystal structure formation as shown in the XRD spectrum. From the FESEM image, the ZnO film is continuous and different size grains to form polycrystalline. The surface morphology properties are rough and the surface is gully shaped and the boundary of the grain blurred. The band gap of the thin film is 3.26 eV by the linear fit of band-edge absorption. PL spectra of the ZnO thin film indicated that the coalescence of small crystals caused the displacement of grain boundaries at 350 °C, leading to the formation of non-radiative recombination centers. The response and recovery

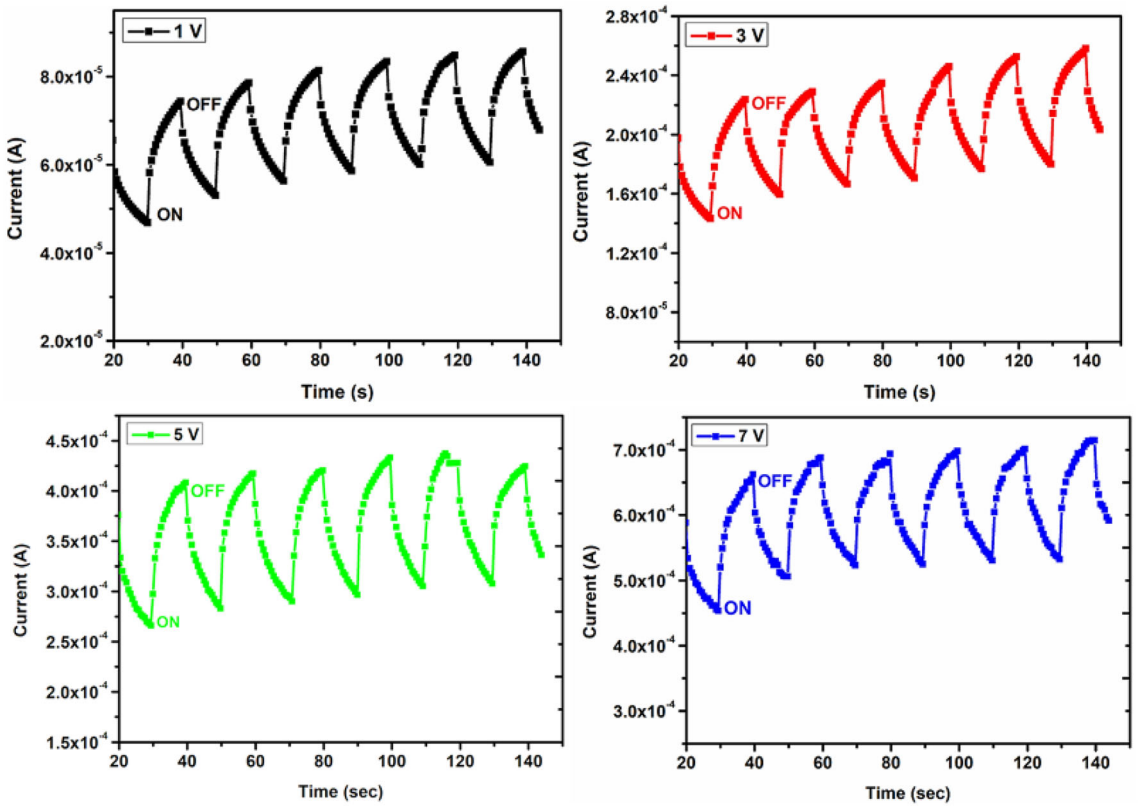

Fig. 8 Response and recovery-current characteristics of fabricated ZnO thin-film sensor

Table 1 Comparison between the literature and the current study of the responsivity and sensitivity for the ZnO thin-film UV photodetector

Materials	Bias voltage (V)	λ (nm)	Responsivity (A/W)	Sensitivity (%)	Response time (s)	Recovery time (s)	Reference
ZnO film	2	390	0.617	10	–	–	[20]
ZnO nanowires	1	370	–	137.5	25	254	[45]
ZnO film	5	365	–	66	18	24	[47]
ZnO nanoparticles	2	365	0.04	4.9×10^3	14.4	33.6	[48]
ZnO nanorods	1	360	0.046	746	89	106	[49]
ZnO nanofibers	2	360	0.00128	2.5×10^4	3.90	4.71	[50]
ZnO tetrapods	5	365	0.917	15.22×10^3	1.4	1.2	[51]
ZnO thin film	5	375	–	800	16	8	[52]
ZnO nanostructures	1	360	0.046	570	89	106	[49]
ZnO/diamond film	10	220	0.004	–	–	–	[53]
ZnO thin film	5	380	4.2	43	3.7	5.3	This work

times of ZnO UV detector are found as 3.7 s and 5.3 s, respectively. The device shows a sensitivity of 43% upon exposure to UV light (0.66 $\mu W/cm^2$) at 5 V and high response peak of 4.3 A/W.

Acknowledgements

The authors thank the staff of the Department of Biophysics, College of Applied Sciences-Hit, in the

University of Anbar. Our gratitude also goes to the Research Creativity and Management Office (RCMO), Universiti Sains University (USM) USM, and to supporting we by the Bridging grant (304.CINOR.6316526).

References

1. X.-T. Yin, P. Lv, J. Li, A. Jafari, Wu. Fa-Yu, Qi. Wang, D. Dastan, Z. Shi, Yu. Shengtao, H. Garmestani, Nanostructured tungsten trioxide prepared at various growth temperatures for sensing applications. J. Alloys Compd. **825**, 154105–154112 (2020)
2. W.-D. Zhou, D. Dastan, X.-T. Yin, S. Nie, Wu. Saisai, Qi. Wang, J. Li, Optimization of gas sensing properties of n-SnO_2/p-x CuO sensors for homogenous gases and the sensing mechanism. J. Mater. Sci.: Mater. Electron. **31**, 18412–18426 (2020)
3. S.A. Kamaruddin et al., Zinc oxide films prepared by sol-gel spin coating technique. Appl. Phys. A **104**, 263–268 (2011)
4. S. Benramache, Y. Aoun, A. Charef, B. Benhaoua, S. Lakel, Transition width effect on optical characterizations of ZnO thin films deposited by spray ultrasonic. Inorg. Nano-Met. Chem. **49**, 177–181 (2019)
5. H. Tian, H. Fan, M. Li, L. Ma, Zeolitic imidazolate framework coated ZnO nanorods as molecular sieving to improve selectivity of formaldehyde gas sensor. ACS Sens. **1**, 243–250 (2016)
6. J. Fang, H. Fan, Y. Ma, Z. Wang, Qi. Chang, Surface defects control for ZnO nanorods synthesized by quenching and their anti-recombination in photocatalysis. Appl. Surf. Sci. **332**, 47–54 (2015)
7. J. Li, H. Fan, X. Jia, Multilayered ZnO nanosheets with 3D porous architectures: synthesis and gas sensing application. J. Phys. Chem. C **114**, 14684–14691 (2010)
8. F.U. Hamelmann, Thin film zinc oxide deposited by CVD and PVD. J. Phys.: Conf Ser. **764**, 12001–12008 (2016)
9. P.Y. Dave, K.H. Patel, K.V. Chauhan, A.K. Chawla, S.K. Rawal, Examination of zinc oxide films prepared by magnetron sputtering. Proc. Technol. **23**, 328–335 (2016)
10. M. Opel, S. Geprägs, M. Althammer, T. Brenninger, R. Gross, Laser molecular beam epitaxy of ZnO thin films and heterostructures. J. Phys. D Appl. Phys. **47**, 3034002–3340028 (2013)
11. J.K. Saha, R.N. Bukke, N.N. Mude, J. Jang, Significant improvement of spray pyrolyzed ZnO thin film by precursor optimization for high mobility thin film transistors. Sci. Rep. **10**, 1–11 (2020)
12. S. Nie, D. Dastan, J. Li, W.-D. Zhou, Wu. Sai-Sai, Y.-W. Zhou, X.-T. Yin, Gas-sensing selectivity of n-ZnO/p-Co_3O_4 sensors for homogeneous reducing gas. J. Phys. Chem. Solids **150**, 109864–109874 (2021)
13. J. Zhang, X. Sun, T. Qi, Ge. Ren, Y. Shan, Q. Dong, Characterization of ZnO films prepared by sol-gel method. AIP Conf. Proc. **1820**, 020002020004 (2017)
14. S. Gong, J. Liu, J. Xia, L. Quan, H. Liu, D. Zhou, Gas sensing characteristics of SnO_2 thin films and analyses of sensor response by the gas diffusion theory. Mater. Sci. Eng. **164**, 85–90 (2009)
15. J.H. Mun, H.J. Lee, S.H. Lee, T.-S. Yoon, S.H. Han, D.H. Kim, Strain-induced photocurrent enhancement in photodetectors based on nanometer-thick ZnO films on flexible polydimethylsiloxane substrates. ACS Appl. Nano Mater. **3**, 10922–10930 (2020)
16. H.K. Yadav, K. Sreenivas, V. Gupta, Study of metal/ZnO based thin film ultraviolet photodetectors: the effect of induced charges on the dynamics of photoconductivity relaxation. J. Appl. Phys. **107**, 44507–44516 (2010)
17. S.K. Panda, C. Jacob, Preparation of transparent ZnO thin films and their application in UV sensor devices. Solid-State Electron. **73**, 44–50 (2012)
18. B. Hanna, K.P. Surendran, K.N. Narayanan Unni, Low temperature-processed ZnO thin films for p-n junction-based visible-blind ultraviolet photodetectors. RSC Adv. **8**, 37365–37374 (2018)
19. V.D. Pon, K.S. Joseph Wilson, K. Hariprasad, V. Ganesh, H. Elhosiny Ali, H. Algarni, I.S. Yahia, Enhancement of optoelectronic properties of ZnO thin films by Al doping for photodetector applications. Superlattices Microstruct. **151**, 106790–106792 (2021)
20. G.M. Ali, P. Chakrabarti. Fabrication and Performance of UV Photodetector Based on Nanostructure ZnO Thin-Film Deposited by Vacuum Coating Technique. International Conference on Developments of E-Systems Engineering (DeSE), 259–264. IEEE, (2015).
21. A. Echresh, C.O. Chey, M.Z. Shoushtari, V. Khranovskyy, O. Nur, M. Willander, UV photo-detector based on p-NiO thin film/n-ZnO nanorods heterojunction prepared by a simple process. J. Alloys Compd. **632**, 165–171 (2015)
22. Ke. Shan, Z.-Z. Yi, X.-T. Yin, L. Cui, D. Dastan, H. Garmestani, F.M. Alamgir, Diffusion kinetics mechanism of oxygen ion in dense diffusion barrier limiting current oxygen sensors. J. Alloys Compd. **855**, 157465–157476 (2021)
23. X. Gu, M. Zhang, F. Meng, Yu. Xindong Zhang, Chen, and Shengping Ruan., Influences of different interdigital spacing on the performance of UV photodetectors based on ZnO nanofibers. Appl. Surf. Sci. **307**, 20–23 (2014)

24. X.-T. Yin, J. Li, D. Dastan, W.-D. Zhou, H. Garmestani, F.M. Alamgir, Ultra-high selectivity of H2 over CO with a pn nanojunction based gas sensors and its mechanism. Sens. Actuators B Chem. **319**, 128330–128343 (2020)
25. M. Jo, K.J. Lee, S.S. Yang, Sensitivity improvement of the surface acoustic wave ultraviolet sensor based on zinc oxide nanoparticle layer with an ultrathin gold layer. Sens. Actuators A **210**, 59–66 (2014)
26. T.K. Pathak, R. Kumar, L.P. Purohit, Preparation and optical properties of undoped and nitrogen doped ZnO thin films by RF sputtering. Int. J. Chem. Technol. Res. **7**, 987–993 (2015)
27. Y. Natsume, H. Sakata, Zinc oxide films prepared by sol-gel spin-coating. Thin Solid Films **372**, 30–36 (2000)
28. U. Chaitra, D. Kekuda, K. Mohan Rao, Effect of annealing temperature on the evolution of structural, microstructural, and optical properties of spin coated ZnO thin films. Ceram. Int. **43**, 7115–7122 (2017)
29. Y.M. Hunge, M.A. Mahadik, A.V. Moholkar, Bhosale CH Photoelectrocatalytic degradation of phthalic acid using spray deposited stratified WO3/ZnO thin film under sunlight illumination. Appl Surf Sci **420**, 764–772 (2017)
30. D. Dastan, Effect of preparation methods on the properties of titania nanoparticles: solvothermal versus sol-gel. Appl. Phys. A **123**, 1–13 (2017)
31. A. Brif, G. Ankonina, C. Drathen, B. Pokroy, Bio-inspired band gap engineering of zinc oxide by intracrystalline incorporation of amino acids. Adv. Mater. **26**, 477–481 (2014)
32. G.-L. Tan, D. Tang, D. Dastan, A. Jafari, Z. Shi, Q.-Q. Chu, J.P.B. Silva, X.-T. Yin, Structures, morphological control, and antibacterial performance of tungsten oxide thin films. Ceram. Int. **47**, 17153–17160 (2021)
33. A. Bedia, F.Z. Bedia, M. Aillerie, N. Maloufi, B. Benyoucef, Morphological and optical properties of ZnO thin films prepared by spray pyrolysis on glass substrates at various temperatures for integration in solar cell. Energy Proc. **74**, 529–538 (2015)
34. S.K. Singh, P. Hazra, S. Tripathi, P. Chakrabarti, Fabrication and experimental characterization of a sol-gel derived nanostructured n-ZnO/p-Si heterojunction diode. J. Mater. Sci.: Mater Electron. **26**, 7829–7836 (2015)
35. G.-L. Tan, D. Tang, D. Dastan, A. Jafari, J.P.B. Silva, X.-T. Yin, Effect of heat treatment on electrical and surface properties of tungsten oxide thin films grown by HFCVD technique. Mater. Sci. Semicond. Proc. **122**, 105506–105512 (2021)
36. F.K. Konan, B. Hartiti, H.J. Tchognia Nkuissi, A. Boko, Optical-structural characteristic of i-ZnO thin films deposited by chemical route. J. Mater. Eviron. Sci. **10**, 1003–1010 (2019)
37. J. Li, H. Fan, X. Jia, J. Chen, Z. Cao, X. Chen, Electrostatic spray deposited polycrystalline zinc oxide films for ultraviolet luminescence device applications. J. Alloys Compd. **481**, 735–739 (2009)
38. M. Peres, S. Magalhães, M.R. Soares, M.J. Soares, L. Rino, E. Alves, K. Lorenz, M.R. Correia, A.C. Lourenço, T. Monteiro, Disorder induced violet/blue luminescence in RF-deposited ZnO films. Phys. Status Solid. c **10**, 662–666 (2013)
39. J. Zhang, X. Sun, T. Qi, Ge. Ren, Y. Shan, Q. Dong, Characterization of ZnO films prepared by sol-gel method. AIP Conf. Proc. **1820**, 020002–020006 (2017)
40. Z. Bi, X. Yang, J. Zhang, X. Bian, D. Wang, X. Zhang, X. Hou, A back-illuminated vertical-structure ultraviolet photodetector based on an RF-sputtered ZnO film. J. Electron. Mater. **38**, 609–612 (2009)
41. L. Hu, M. Chen, W. Shan, T. Zhan, M. Liao, X. Fang, Hu. Xinhua, Wu. Limin, Stacking-order-dependent optoelectronic properties of bilayer nanofilm photodetectors made from hollow ZnS and ZnO microspheres. Adv. Mater. **24**, 5872–5877 (2012)
42. N.K. Hassan, M.R. Hashim, Flake-like ZnO nanostructures density for improved absorption using electrochemical deposition in UV detection. J. Alloys Compd. **577**, 491–497 (2013)
43. S.S. Shinde, K.Y. Rajpure, Fabrication and performance of N-doped ZnO UV photoconductive detector. J. Alloys Compd. **522**, 118–122 (2012)
44. L. Luo, Y. Zhang, S.S. Mao, L. Lin, Fabrication and characterization of ZnO nanowires based UV photodiodes. Sens. Actuators, A **127**, 201–206 (2006)
45. H. Zhang, A.V. Babichev, G. Jacopin, P. Lavenus, F.H. Julien, AYu. Egorov, J. Zhang, T. Pauporté, M. Tchernycheva, Characterization and modeling of a ZnO nanowire ultraviolet photodetector with graphene transparent contact. J. Appl. Phys. **114**, 234505–234514 (2013)
46. Z. Zheng, L. Gan, H. Li, Y. Ma, Y. Bando, D. Golberg, T. Zhai, A fully transparent and flexible ultraviolet-visible photodetector based on controlled electrospun ZnO-CdO heterojunction nanofiber arrays. Adv. Func. Mater. **25**, 5885–5894 (2015)
47. S.K. Shaikh, V.V. Ganbavle, S.I. Inamdar, K.Y. Rajpure, Multifunctional zinc oxide thin films for high-performance UV photodetectors and nitrogen dioxide gas sensors. RSC Adv. **6**, 25641–25641 (2016)
48. M.-S. Choi, T. Park, W.-J. Kim, J. Hur, High-performance ultraviolet photodetector based on a zinc oxide nanoparticle@ single-walled carbon nanotube heterojunction hybrid film. Nanomaterials **10**, 395–411 (2020)

49. S.-J. Young, Y.-H. Liu, N.I. Shiblee, K. Ahmed, L.-T. Lai, L. Nagahara, T. Thundat et al., Flexible ultraviolet photodetectors based on one-dimensional gallium-doped zinc oxide nanostructures. ACS Appl. Electron. Mater. **2**, 3522–3529 (2020)
50. Yi. Ning, Z. Zhang, F. Teng, X. Fang, Novel transparent and self-powered UV photodetector based on crossed ZnO nanofiber array homojunction. Small **14**, 1703754 (2018)
51. F.H. Alsultany, Z. Hassan, N.M. Ahmed, Low-power UV photodetection characteristics of ZnO tetrapods grown on catalyst-free glass substrate. Sens. Actuators A **250**, 187–194 (2016)
52. S.I. Inamdar, K.Y. Rajpure, High-performance metal–semiconductor–metal UV photodetector based on spray deposited ZnO thin films. J. Alloys Compd. **595**, 55–59 (2014)
53. R. Su, Z.C. Liu, X.H. Chang, Y. Liang, G.Q. Chen, X.L. Yan, F.N. Li et al., Characterization of UV photodetector based on ZnO/diamond film. Opt Exp **27**, 36750–36756 (2019)
54. M. Birkholz, *Thin Film Analysis by X-Ray Scattering* (Wiley, New York, 2006)

Terms and Conditions

Springer Nature journal content, brought to you courtesy of Springer Nature Customer Service Center GmbH (“Springer Nature”).
Springer Nature supports a reasonable amount of sharing of research papers by authors, subscribers and authorised users (“Users”), for small-scale personal, non-commercial use provided that all copyright, trade and service marks and other proprietary notices are maintained. By accessing, sharing, receiving or otherwise using the Springer Nature journal content you agree to these terms of use (“Terms”). For these purposes, Springer Nature considers academic use (by researchers and students) to be non-commercial.
These Terms are supplementary and will apply in addition to any applicable website terms and conditions, a relevant site licence or a personal subscription. These Terms will prevail over any conflict or ambiguity with regards to the relevant terms, a site licence or a personal subscription (to the extent of the conflict or ambiguity only). For Creative Commons-licensed articles, the terms of the Creative Commons license used will apply.
We collect and use personal data to provide access to the Springer Nature journal content. We may also use these personal data internally within ResearchGate and Springer Nature and as agreed share it, in an anonymised way, for purposes of tracking, analysis and reporting. We will not otherwise disclose your personal data outside the ResearchGate or the Springer Nature group of companies unless we have your permission as detailed in the Privacy Policy.
While Users may use the Springer Nature journal content for small scale, personal non-commercial use, it is important to note that Users may not:

1. use such content for the purpose of providing other users with access on a regular or large scale basis or as a means to circumvent access control;
2. use such content where to do so would be considered a criminal or statutory offence in any jurisdiction, or gives rise to civil liability, or is otherwise unlawful;
3. falsely or misleadingly imply or suggest endorsement, approval , sponsorship, or association unless explicitly agreed to by Springer Nature in writing;
4. use bots or other automated methods to access the content or redirect messages
5. override any security feature or exclusionary protocol; or
6. share the content in order to create substitute for Springer Nature products or services or a systematic database of Springer Nature journal content.

In line with the restriction against commercial use, Springer Nature does not permit the creation of a product or service that creates revenue, royalties, rent or income from our content or its inclusion as part of a paid for service or for other commercial gain. Springer Nature journal content cannot be used for inter-library loans and librarians may not upload Springer Nature journal content on a large scale into their, or any other, institutional repository.
These terms of use are reviewed regularly and may be amended at any time. Springer Nature is not obligated to publish any information or content on this website and may remove it or features or functionality at our sole discretion, at any time with or without notice. Springer Nature may revoke this licence to you at any time and remove access to any copies of the Springer Nature journal content which have been saved.
To the fullest extent permitted by law, Springer Nature makes no warranties, representations or guarantees to Users, either express or implied with respect to the Springer nature journal content and all parties disclaim and waive any implied warranties or warranties imposed by law, including merchantability or fitness for any particular purpose.
Please note that these rights do not automatically extend to content, data or other material published by Springer Nature that may be licensed from third parties.
If you would like to use or distribute our Springer Nature journal content to a wider audience or on a regular basis or in any other manner not expressly permitted by these Terms, please contact Springer Nature at

onlineservice@springernature.com